TSUNAMI RUNUP AMPLIFICATION OF BREAKING AND NON-BREAKING ERROR-FUNCTION WAVES OVER A SLOPING BEACH IN SHADOW ZONE BY A SAMLL ISLAND

Sunghoon Han¹, James M. Kaihatu¹, Patrick J. Lynett², and Costas E. Synolakis²

The time series of free surface elevation measured in and outside the shadow zone were compared and analyzed in the time-frequency domain by employing the continuous wavelet transform. Regardless of the conditions of the ERF wave in the shadow zone, an increase in magnitude of energy is noticeable not only in the peak frequency within a range of approximately 0.8 to 1 Hz but also in the low-frequency range of around 0.1 Hz corresponding to second up to third crest of the leading wave. To determine the effective frequency of ERF waves and evaluate their runup characteristics, we applied a new method of describing the ERF wave, which consists of linear superposition of two solitary waves. As a result, the ERF waves show the same trend in runup characteristics as for solitary waves.

Keywords: tsunami; runup; wavelet transform; error function wave; effective frequency

INTRODUCTION

The Mentawais tsunami of 2010 was unusual in that it highlighted the effect of islands on the tsunami inundation of beaches in the shadow zones behind them. Post-tsunami surveys of shorelines in the lee of offshore islands showed tsunami runup amplification (TRA), a higher degree of inundation relative to open coastal shorelines. This is in direct opposition to widely-held beliefs of the local population regarding the sheltering effects of islands.

Experiments of tsunami wave propagation around conical islands conducted at the Directional Wave Basin at Oregon State University revealed that, in general, there was an inverse relationship between island distance to the shoreline and the TRA with non-breaking error-function (ERF) waves. However, a noticeable phenomenon we found is that a breaking ERF wave (a tsunami propagating as a dissipative bore prior to reaching the island) results in a directly proportional relationship between the quantities in question.

Through the experiments, the TRA phenomenon of the ERF wave caused by the island was observed, but it is difficult to specify a geometric scale that can be linked to the topographic features of the island and shadow zone for long transient waves such as ERF waves.

In this study, we analyze how the ERF wave passing through the island changes in the frequency-time domain using wavelet transform, which is useful for nonstationary signal analysis (Lee. and Yamamoto 1994). And to understand the relationship between the geometric characteristics of ERF and the maximum runup, a new effective frequency is obtained and the runup statistic in terms of surf-similarity is compared with the trend of the solitary wave.

EXPERIMENT DATA

The ERF wave was generated by the wavemaker with given by an error function of varying stroke period. 5 sec ERF (ERF5s) wave has shortest length but highest amplitude and is broken before reaching the island. The other ERF (ERF8s, 10s, and 12s) wave is non-breaking wave. For more information on the physical properties of ERF waves, refer to Baldock et al. 2009.

Fig. 1 is a schematic diagram showing the arrangement of wave gauges that will be under discussion in the following sections. The length of shadow zone (LOS) which is dependent on the location of the island is defined a metrical distance from the beach toe to the base of the island. BI and BN location in x-direction is varying with the LOS. As shown in the Fig. 2, Even if the same ERF wave passes through an island of the same size, it can be seen that the wave height and duration of the leading and trailing wave passing through the in-shadow zone vary significantly depending on the distance of the island (depending on the LOS).

The effect of these differences on runup amplification requires a three-dimensional analysis of the nonlinear interaction of two refracted waves passing through the island. This will be the subject of future research. Representatively, this paper deals with the change in frequency of non-breaking and breaking ERF for only 8-LOS case.

¹ Zachry Department of Civil & Environmental Engineering, Texas A&M University, College Station, TX, 77840, USA

² Sonny Astani Department of Civil & Environmental Engineering, University of Southern California, Los Angeles, CA, USA

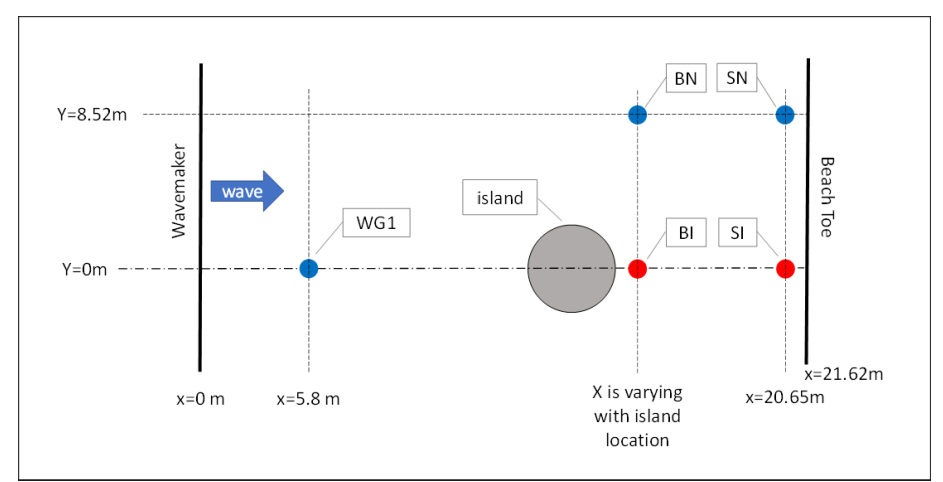


Figure 1. Arrangement of wave gauges: before reaching the island (WG1), the in-shadow zone (BI & SI), and the no-shadow zone (BN & SN), water depth: 0.5 m, the conical island: 1m height, 4m diameter of its base.

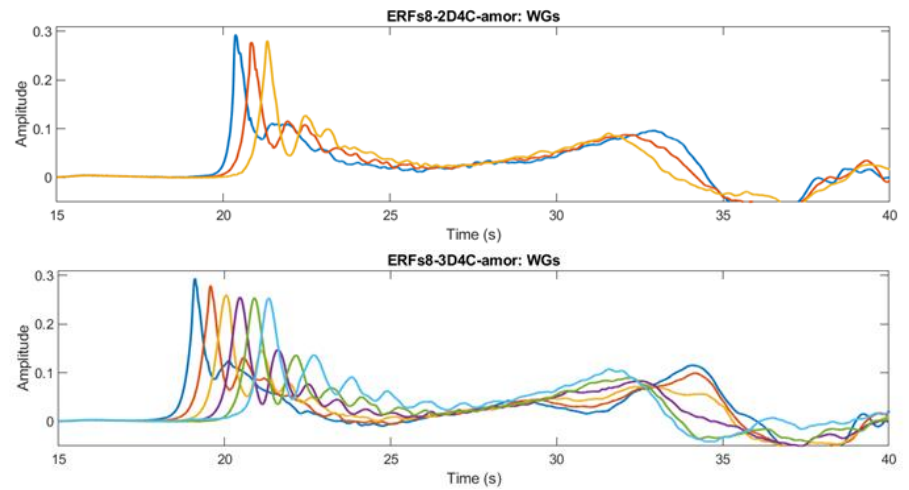


Figure 2. Time series of surface elevation of ERF8s along the centerline in 4-LOS (above) and 8-LOS (below), respectively, different color means different location of gauges between BI and SI.

WAVELET TRANSFORM (NON-BREAKING ERF WAVE)

In this section, we applied the wavelet transform in an attempt to investigate the effect of a small island to the shadow zone. By performing the continuous wavelet transform (CWT) of the signal $\eta(t)$ as function of scale p and shift q (as shown Eq. 1) with the complex Morlet wavelet (as shown Eq. 2), the wavelet spectrogram for the signal can be given as a function of magnitude of coefficients in time and frequency domain.

$$X_{\text{cwt}}(p,q) = \frac{1}{\sqrt{p}} \int_{-\infty}^{\infty} \eta(t) \, \varphi(\frac{t-q}{p}) dt$$
 (1)

$$\varphi(t) = A \frac{1}{\sqrt{\pi}} e^{2\pi i t} e^{-t^2} \tag{2}$$

where A is a normalization constant. The calculations were performed using the wavelet toolbox of MATLAB (Misiti et al. 2020).

Fig. 3 shows time series of surface elevation and corresponding spectrograms measured at the five gauges shown in Fig. 1. The time series of WG1 shows an asymmetric leading wave and a following long-duration hump, but we do not consider the hump in this study because we are interested only in the leading wave which is a major part of causing the maximum runup on the beach slope, also the hump could be affected by the reflection wave from the wavemaker.

Basically, the time series shows the increase in the amplitude of the leading wave at both the inshadow zone (BI & SI, red solid line) and the no-shadow zone (BN & SN, blue solid line) comparing

to WG1. As the ERF wave is propagating, dispersion occurs on the descending side of the leading wave and then second and third crest appear on that side while the amplitude of the first crest increases.

When comparing between the in- and no-shadow zone, the ERF wave tends to have a slightly higher the second or third crest as well as the first crest in the shadow zone. This difference is also evident in the frequency-time domain; the spectrograms of the in-shadow zone represent that the energy concentration for the leading wave increases considerably around $0.8 \sim 1.0$ Hz. On the other hand, the energy distribution of low frequency (around 0.1 Hz) for the second and third crest whose time range is from peak-time to around 25 sec is higher than that of the no-shadow zone case.

The high frequency component on the sagging part following the leading wave is found in the noshadow zone. This is thought it is because of the reflection wave from the island.

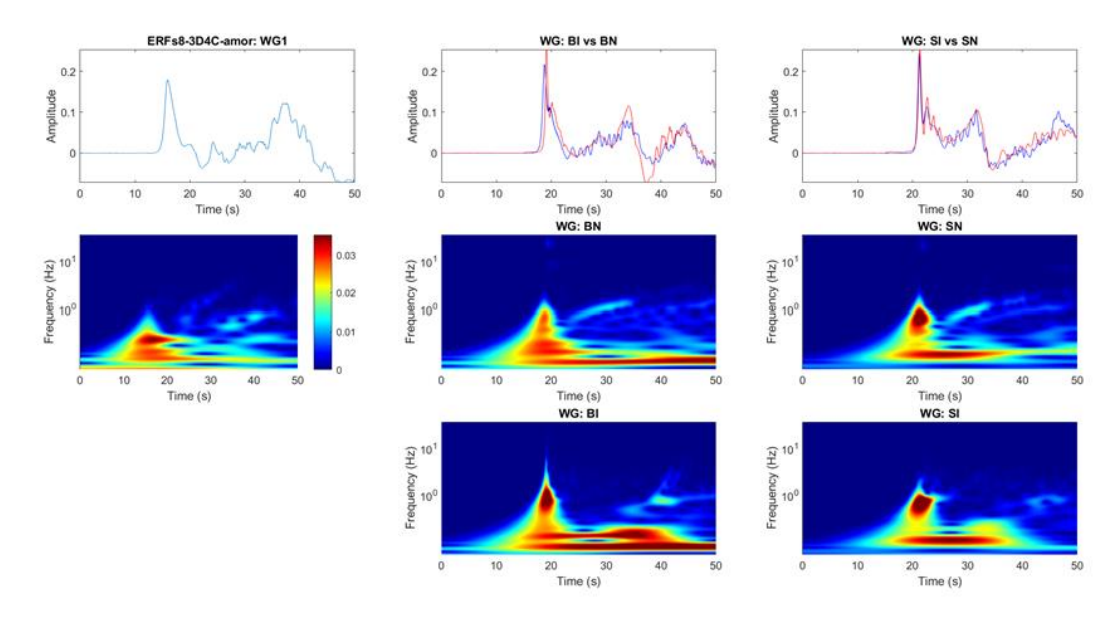


Figure 3. Time series of surface elevation (first row), and corresponding spectrograms (second and third row) of ERF8s in 8-LOS at WG1 (first column), BN & BI (second column), and SN & SI (third column)

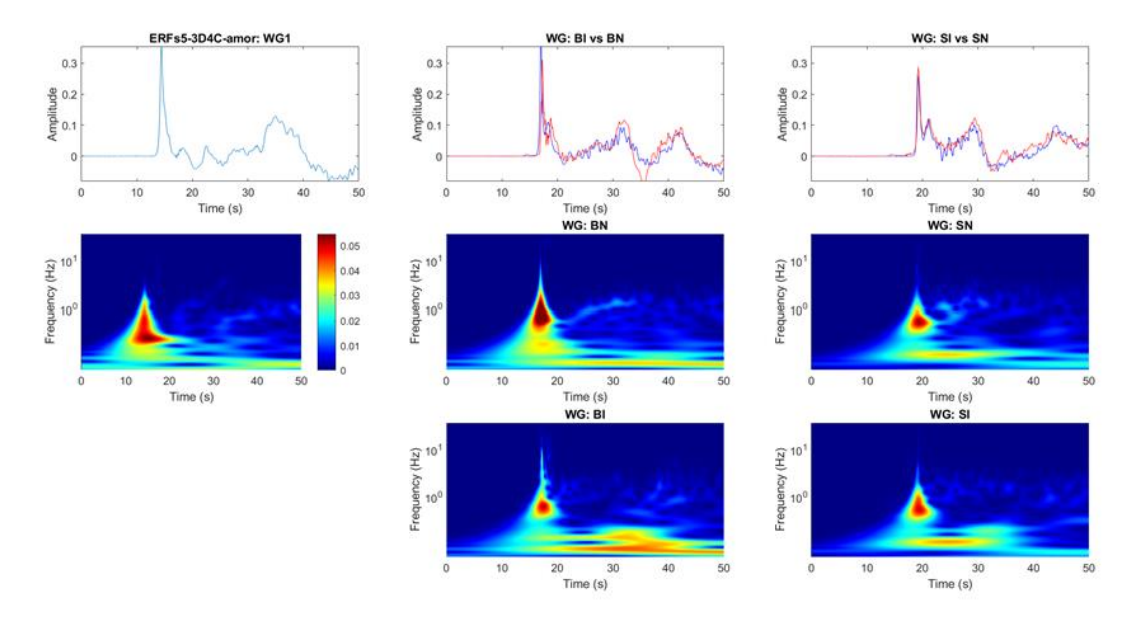


Figure 4. Time series of surface elevation (first row) and corresponding spectrograms (second and third row) of ERF5s in 8-LOS at WG1 (first column), BN & BI (second column), and SN & SI (third column)

WAVELET TRANSFORM (BREAKING ERF WAVE)

The ERF5s wave is broken right before reaching the island then maintains the fully bored condition until finish the runup process on the sloping beach. So, as shown in Fig. 4, when the dissipative wave reaches SI or SN (x = 20.65 m), the leading amplitude decreases, unlike the non-breaking case. However, the energy distribution of low-frequency (around 0.1 Hz) for the second crest in the shadow zone still has higher than the no-shadow zone like as non-breaking wave case.

Given the above results both non-breaking and breaking cases, not only the increase of the amplitude of first crest of the leading wave but also the increase of the energy of the second up to third crest can be considered as a factor affecting runup amplification.

Thus, in the following section, we can define an effective frequency for the ERF wave considering the second up to third crest to find out the relationship between maximum inundation depth and geometric scale.

EFFECTIVE FREQUENCY OF ERF WAVE

Unlike solitary wave, it is hard to characterize ERF wave which is an evolving long-transient wave in geometric scale. However, when the wave reaches the near the beach toe, due to the dispersion of the leading wave, it is possible to approximately describe the leading elevation of ERF wave by overlapping several solitary waves as shown in Fig. 5. This linear overlapping two successive solitary waves has been studied by Chan and Liu (2012). They extended the analytical solutions by Madsen and Schaffer (2010) for the shoreline solutions of multiple solitary waves.

In this section we suggest a new way to get a geometric effective frequency for ERF wave by summing the frequencies of each solitary wave. The approximation describing ERF wave with two successive solitary waves is obtained as

$$\eta(t) = A_1 \operatorname{sech}^2 [\Omega_1(t - t_1)] + A_2 \operatorname{sech}^2 [\Omega_2(t - t_2)]$$
(3)

where $A_2 = \mu A_1$ and $\Omega_2 = \sqrt{\mu}\Omega_1$ with μ is the amplitude ratio, and $\Omega_1 = (1/h)\sqrt{3A_1/4h}\sqrt{g(h+A_1)}$. t_1 and t_2 are phase shifts. Assuming that each solitary wave can be an isosceles triangle approximately and have each frequency corresponding to its amplitude as shown in Fig. 5, we define $\omega_1 = \frac{\Omega_1}{2} \frac{V}{A_1}$ and $\omega_2 = \frac{\Omega_2}{2} \frac{V}{A_2}$ as the frequencies associated with the intersection areas, VCB_1 and VCB_2 , respectively, as shown in the first panel of Fig. 5.

In such intuitive way, we derived Eq. 4 as the effective frequency of ERF by subtracting the intersect frequencies from the frequencies of the two solitary waves.

$$\Omega_{ERF} = \Omega_1 + \Omega_2 - \frac{V}{2} \left(\frac{\alpha_1}{A_1} + \frac{\alpha_2}{A_2} \right) \tag{4}$$

Similar way, the effective frequency consists of three solitary waves can be obtained as

$$\begin{split} \Omega_{ERF} &= \Omega_1 + \Omega_2 + \Omega_3 - (\omega_l + \omega_r) \\ &= \Omega_1 + \Omega_2 + \Omega_3 - \frac{1}{2} \left[\frac{V_1}{A_1} \Omega_1 + \frac{(V_1 + V_2)}{A_2} \Omega_2 + \frac{V_2}{A_2} \Omega_3 \right] \end{split} \tag{5}$$

where $\omega_l = \frac{\Omega_1}{2} \frac{V_1}{A_1} + \frac{\Omega_2}{2} \frac{V_1}{A_2}$ and $\omega_r = \frac{\Omega_3}{2} \frac{V_2}{A_3} + \frac{\Omega_2}{2} \frac{V_2}{A_2}$ indicate the first and second intersect frequencies, respectively, as shown in the second panel of Fig. 5.

Fig. 6 shows comparisons of ERF 5s, 8s, 10s, and 12s with its composite solitary wave result from the Eq. 4 and 5. When a third or fourth solitary wave was added in addition to the composite solitary wave depicted in Fig. 6, the total effective frequency (Ω_{ERF}) did not change significantly. Because as the amplitude of crest decreases, the corresponding frequency decreases, so the effect of the addition solitary wave on the total effective frequency decreases. So, the following section, we will apply each effective frequency suggested by Eq. 4 and 5 into the runup statistics in terms of surf-similarity.

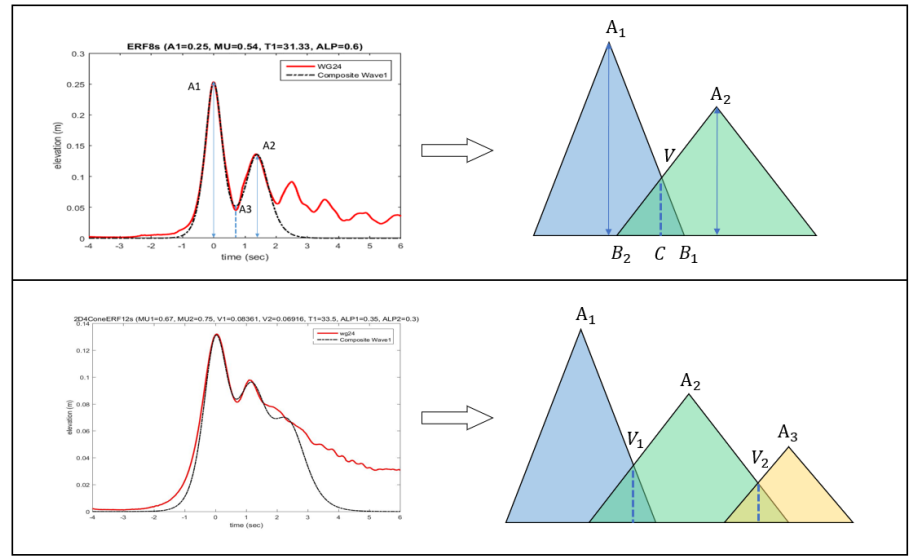


Figure 5. The overlapped waves simplified into two or three isosceles triangles; red solid line: time series of data of ERF8s (above) and ERF12s (below), black dash-dot line: overlapped solitary wave, A: amplification of solitary wave, V: minimum elevation between two near crests.

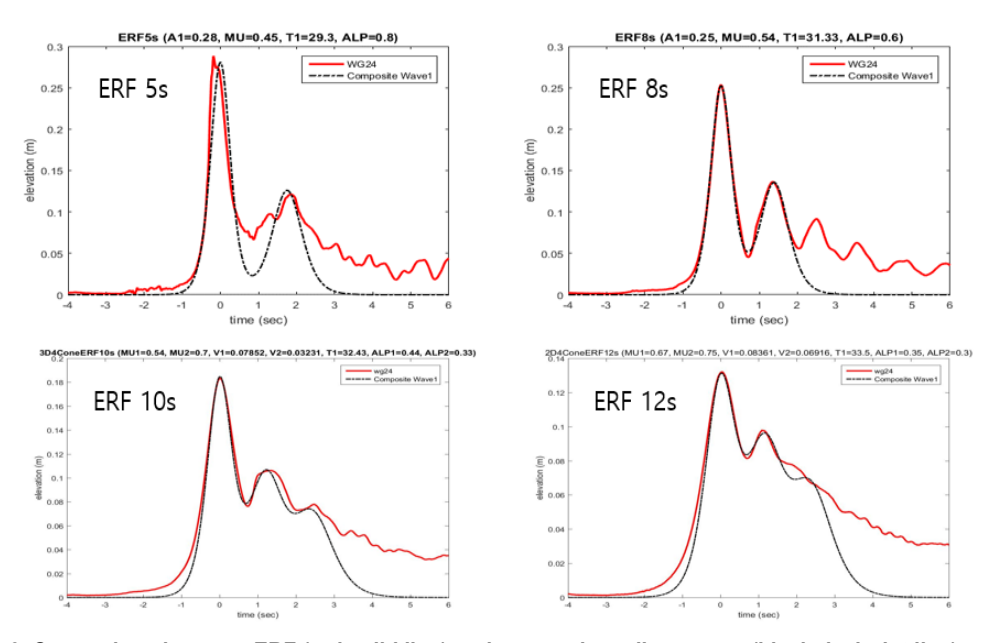


Figure 6. Comparison between ERF (red solid line) and composite solitary wave (black dash-dot line)

RUNUP STATISTICS IN TERMS OF SURF SIMILARITY

To confirm the adequacy of ERF's effective frequency using the Eq. 4 and 5, it was compared with runup statistics of solitary wave. The left comparison of Fig. 7 represents runup statistics in terms of surf-similarity (ξ_1) which is related to only the first crest of the leading wave, but the right plot was compared with surf-similarity associated with the effective frequency (Ω_{ERF}) rather than the frequency for the first crest (Ω_1).

As shown in the right comparison of Fig. 7, the ERF case shows the almost same trends as the solitary shows. That implies that the effective frequency using the linear superposition of multiple solitary waves can be used to characterize the ERF wave in the geometric scale by considering the second and third crest when it comes to the maximum inundation depth.

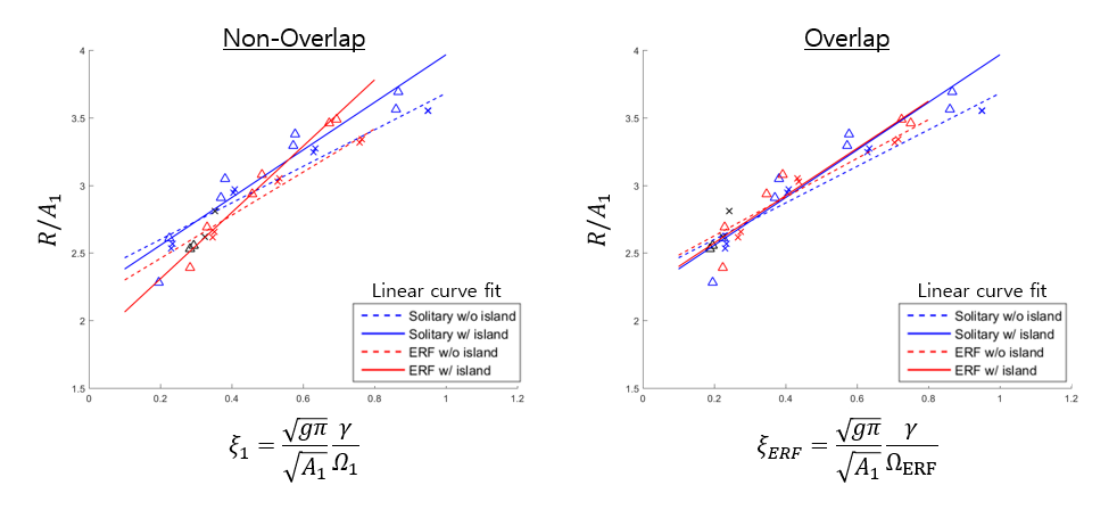


Figure 7. maximum runup statistics in terms of surf-similarity; triangle: the in-shadow zone, x: the no-shadow zone, red: non-breaking ERF wave, blue: solitary wave, black: breaking ERF wave, solid line: linear curve fit of the same color marker in the shadow zone, dash line: linear curve fit of the same color marker out of the shadow zone.

CONCLUSIONS

We employed the continuous wavelet transform technique to investigate how the non-breaking and breaking ERF wave changes in the frequency-time domain by passing a small offshore island. ERF wave tends to have higher energy concentration in both ranges of high-frequency (0.8-1.0Hz) and low-frequency (around 0.1Hz) than that of the no-shadow zone. Through the wavelet transform results we can conclude the implication that the second up to third crest is not negligible in terms of the effect of shadow zone on TRA.

Although the ERF wave is an evolving transient wave, when it reaches the beach toe, the leading wave related to the maximum inundation depth on the sloping beach can be described by overlapping with multiple solitary waves. So, we presented a method of obtaining the frequency of ERF's leading wave by an intuitive geometric method of summing the frequencies of successive solitary waves and subtracting the overlapping part.

As a result of comparing the runup statistics for solitary wave by applying the effective frequency obtained in such way to surf similarity for ERF waves, the runup statistics for the ERF wave is almost equivalent to the runup trends of the solitary wave.

Therefore, it is expected that TRA trends can be analyzed by linking the geometrical scale of the ERF wave and the topographical features of the island diameter or of the LOS.

ACKNOWLEDGMENTS

This study was supported by CMMI Directorate Award 1538190 from National Science Foundation

REFERENCES

Baldock, T. E., Cox, D., Maddux, T., Killian, J., and Fayler, L. (2009). Kinematics of breaking tsunami wavefronts: A data set from large scale laboratory experiments. Coastal Engineering, 56(5-6), 506-516.

Chan, I. C., and Liu, P. L. F. (2012). On the runup of long waves on a plane beach. Journal of Geophysical Research: Oceans, 117(C8).

Lee, D. T., and Yamamoto, A. (1994). Wavelet analysis: theory and applications. Hewlett Packard journal, 45, 44-44.

Madsen, P. A., and Schaeffer, H. A. (2010). Analytical solutions for tsunami runup on a plane beach: single waves, N-waves and transient waves. Journal of Fluid Mechanics, 645, 27.

Misiti, M., Y. Misiti, G. Oppenheim, and J. Poggi (2020), Wavelet toolbox user's guide, MathWorks, Inc., Natick, Mass